Supplementary Information

Design principles, growth laws, and competition of minimal autocatalysts

Yann Sakref & Olivier Rivoire

Contents

1 Model

Our model consists of Brownian particles with isotropic or anisotropic interactions. The model is general, but setting our parameter values, we choose them to describe experiments with DNA-coated colloids, which are a possible experimental realization of our model. To capture all relevant physical trade-offs of (auto)catalysis, we fit the (auto)catalysis mediated by these particles by a Markov model calibrated to reproduce the results of molecular dynamics (MD) simulations. In this section, we detail the definition of the model, the MD simulations, and the construction of the Markov model.

1.1 Physical model

We consider spherical particles of diameter σ subjected to Brownian dynamics. We fix $\sigma = 1$ for the length scale of the system, $k_BT = 1$ for the energy scale, and take $\gamma = 10$ for the damping constant, which results in a translational diffusion coefficient $D = k_BT/\gamma = 0.1$ length^2/time, comparable to values measured experimentally with colloids [1].

The potential by which the particles interact is a generalization of the isotropic pairwise Wang-Frenkel potential [2], with a cutoff value of $r_c = 1.1$, represented by

$$\phi(r) = \begin{cases} \alpha\left(r_\mathrm{c}\right)\left[\left(\frac{\sigma}{r}\right)^2 - 1\right]\left[\left(\frac{r_\mathrm{c}}{r}\right)^2 - 1\right]^2 & \text{for } r \le r_\mathrm{c} \\ 0 & \text{for } r > r_\mathrm{c} \end{cases}, \tag{S1}$$

where

$$\alpha\left(r_\mathrm{c}\right) = 2\left(\frac{r_\mathrm{c}}{\sigma}\right)^2\left(\frac{3}{2\left(\left(\frac{r_\mathrm{c}}{\sigma}\right)^2 - 1\right)}\right)^3 \qquad \text{and} \qquad r_\mathrm{min}\left(r_\mathrm{c}\right) = r_\mathrm{c}\left(\frac{3}{1 + 2\left(\frac{r_\mathrm{c}}{\sigma}\right)^2}\right)^{1/2}. \tag{S2}$$

This potential has proven to be a good model for interactions involving DNA-coated colloids [3]. We introduce a reaction barrier by adding a mirrored reflection of this potential along the ϵ^-_{AA}-axis, with a maximum at $r = 1.1\ \sigma$, and a cutoff at $r_c = 1.17\ \sigma$.

Formally, the potential between two particles ϵ^-_{AA} and Y is taken to be

$$U_{XY}(r) = \begin{cases} \epsilon^-_{XY}\phi\left(r\right) + \epsilon^+_{XY} & r \le r_\mathrm{c} \\ -\epsilon^-_{XY}\phi\left(r - r_\mathrm{c} + r_\mathrm{min}\right) & r_\mathrm{c} \le r \le 2r_\mathrm{c} - r_\mathrm{min} \end{cases} \tag{S3}$$

where ϵ^-_{XY} and ϵ^+_{XY} represent the activation barriers for dissociation and association, respectively (Fig. 1B).

1.2 Molecular dynamics simulations

Molecular dynamics simulations were carried out in HoomD 3.5.0 [4], using a time step $\Delta t = 10^{-5}$ and periodic boundary conditions.

When considering anisotropic particles, we use the rigid bodies simulations implemented in HoomD [5, 6]. A rigid body is composed of a large inert particle with a diameter of σ, to which smaller particles, each with a diameter of 0.1σ, are arranged on its surface. These smaller particles define patches that interact with each other via the potential given in Eq. (S3) where $r_\mathrm{min} = 0.03\sigma$, $r_c = 0.1$ if $\epsilon^+_{XY} = 0$, and $r_\mathrm{max} = 0.1$ and $r_c = 0.117$ otherwise. These parameters are such that the equilibrium distance between two large particles remains $1.03\ \sigma$.

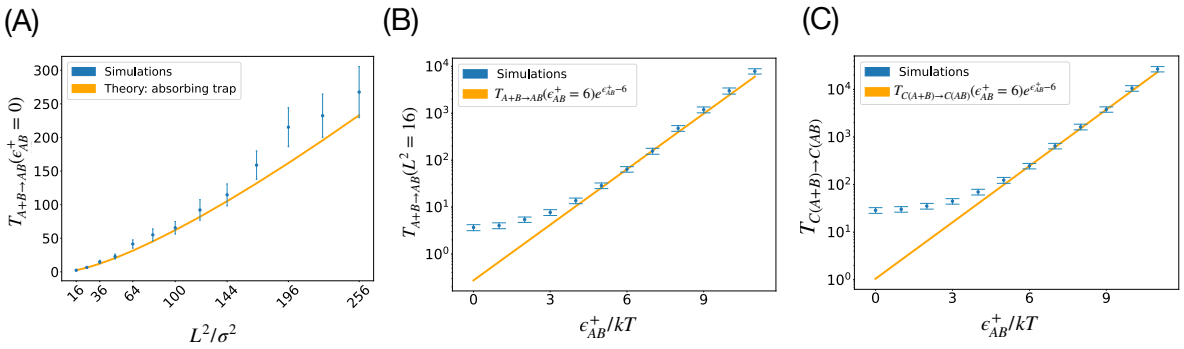

Figure S1: Dimerization reactions in the bulk and on the (auto)catalyst. **(A)** In blue, molecular dynamics (MD) simulation results of the time required for two particles, initially placed randomly within a reaction area L^2, to diffuse toward each other. The orange line is the theoretically calculated first passage time of a particle confined within a disk of radius $L/2$ reaching an absorbing trap of radius $\sigma/2$ at the center of the disk [7]. **(B)** Mean dimerization time in the bulk $T_{A+B\to AB}$ as a function of the energy barrier ϵ^+_{AB}. We verify Arrhenius law for sufficiently large ϵ^+_{AB}, specifically at the value $\epsilon^+_{AB} \gtrsim 6\ k_BT$. **(C)** Mean dimerization time on the autocatalyst $T_{AB(A+B)\to AB(AB)}$, as a function of the energy barrier ϵ^+_{AB}, which verifies again Arrhenius law for $\epsilon^+_{AB} \gtrsim 6\ k_BT$.

1.3 Markov models

In this section, we present how a Markov model is built to reproduce the dynamics observed in MD simulations. It is obtained by analyzing each step of the cycle shown in Fig. 1A of the main text, from binding to release, and applies to both an autocatalyst AB and a catalyst $C = A'B'$, hereinafter collectively referred to as C for the sake of generality.

First, we approximate the mean dimerization time in the absence of catalyst by Arrhenius equation [8] as $T_{A+B\to AB} \approx T_d e^{\epsilon^+_{AB}}$, where T_d refers to the average time needed for two particles randomly placed in the reaction area L^2 to come in contact. As shown in Fig. S1A, this time T_d is well approximated by the mean first-passage time taken by a point-like particle confined within a disk of radius $R_d = L\pi^{-1/2}$ to reach an absorbing trap of radius $R_t = 2\sigma$ at the center of the disk [7].

The exponential scaling of $T_{A+B\to AB}$ with ϵ^+_{AB} is also verified for sufficiently large values of ϵ^+_{AB} (Fig. S1B). However, while T_d is a good approximation for two randomly placed particles to first diffuse towards each other, it does not adequately account for the succession of unbinding and rebinding events. Indeed, a particle is more likely to (re)bind a target when it starts in its vicinity. Therefore, we estimate with the MD simulations the mean time required for rebinding, $T_{d'}$, as a function of L^2. We then use $T_{d'}$ as a substitute for T_d.

To describe the mean reaction time on a (auto)catalyst, we replace $T_{d'}$ by T_c, the average time for the substrates to encounter when constrained to remain bound to the (auto)catalyst. As shown in Fig. S1C, we verify that $T_{C(A+B)\to C(AB)} \approx T_c e^{\epsilon^+_{AB}}$ for sufficiently large ϵ^+_{AB}, consistent with Arrhenius law.

To describe the mean time for a product AB to dissociate from a (auto)catalyst, we first verify that the release of a single monomer scales exponentially with the interaction strength ϵ^-_{AA} (Fig. S2A), consistent again with Arrhenius equation. We model product release as a mean first passage time from the state $C(AB)$ to $C + AB$ via a state $C{\cdot}AB$ in which only one particle of the dimer interacts with the (auto)catalyst. In state $C{\cdot}AB$, the likelihood that a detached particle reattaches before the other particle detaches is high, due to its close proximity with the (auto)catalyst. This likelihood can be calculated as a $1D$ diffusion problem [9] (Fig. S2B, orange line). At high interaction strength ϵ^-_{AA}, the likelihood that a detached particle reattaches before

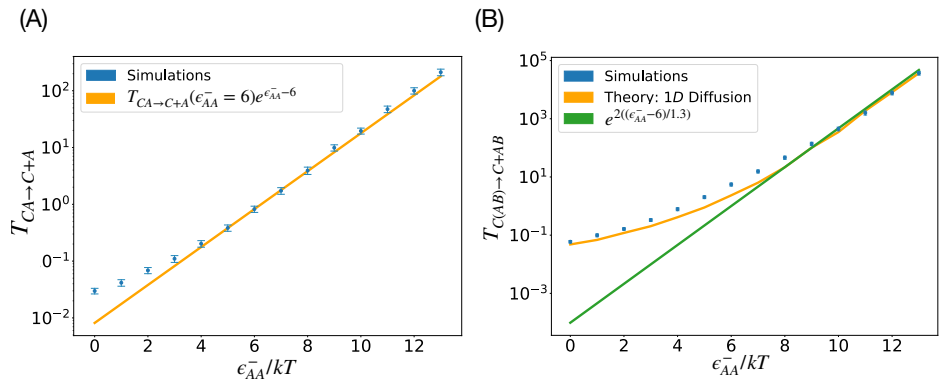

Figure S2: Release of one substrate and of the product from the (auto)catalyst **(A)** Mean release time of a substrate $T_{CA\to C+A}$ as a function of the interaction energy ϵ^-_{AA}. We verify Arrhenius law for sufficiently large ϵ^-_{AA}, specifically when $\epsilon^-_{AA} \gtrsim 6\ k_BT$. **(B)** Mean release time of a product $T_{C(AB)\to C+AB}$ as a function of the interaction energy ϵ^-_{AA}. For low values of ϵ^-_{AA}/k_BT, the mean release time can be computed by considering an intermediate state $C{\cdot}AB$ from which the likelihood – calculated as a $1D$ diffusion problem [9] – that a detached particle reattaches before the other particle detaches is high. For large values of ϵ^-_{AA}/k_BT, the mean time for product release is well approximated by the time for two particles to detach simultaneously, $T_{C(AB)\to C+AB} \approx (T_{C{\cdot}A\to A+C})^2$.

the other particle detaches is so high that we can approximate product release by a single step $(AB)(AB) \to 2AB$ with rate $e^{-2\epsilon^-_{AA}}$, corresponding to the simultaneous breaking of two bonds of interaction strength ϵ^-_{AA} (Fig. S2B, green line).

Overall, from the mean times for the elementary steps of diffusion, dimerization and release, we define a Markov model, whose fit with the MD simulations is represented in Fig. S3. For low energy barriers ($\epsilon^+_{AB} < 6$, $\epsilon^-_{AA} < 6$), the mean time of those processes are directly taken from the MD simulations. For higher energy barriers, when Arrhenius equation applies, we report the rates in the second column of Table S1.

To simplify the presentation, we analyze in the main text and in Sec. 2 below a simplified model that ignores some of the pre-factors to retain only the dependence on the parameters. The reaction rates of this simplified model are listed in the third column of Table S1. In Sec. 3.3, we verify that our results are largely unaffected by this simplification.

Reactions	Comprehensive Markov model ($\epsilon^+_{AB}, \epsilon^-_{AA} > 6$)	Simplified Markov model
$A+B \to AB$	$e^{\epsilon^+_{AB}-6}/T_{d'}$	$e^{\epsilon^+_{AB}}/L^2$
$A+C \to CA$	$2/T_{d'}$	$2/L^2$
$CA \to A+C$	$0.9e^{\epsilon^-_{AA}-6}$	$e^{\epsilon^-_{AA}}$
$CA+B \to C(A+B)$	$1/T_{d'}$	$1/L^2$
$C(A+B) \to CA+B$	$1.8e^{\epsilon^-_{AA}-6}$	$2e^{\epsilon^-_{AA}}$
$C(A+B) \to C(AB)$	$T_c e^{\epsilon^+_{AB}-6} \approx 266 e^{\epsilon^+_{AB}-6}$	$e^{\epsilon^+_{AB}}$
$C(AB) \to C+AB$	$0.81e^{2(\epsilon^-_{AA}-6)/1.3}$	$e^{2\epsilon^-_{AA}}$

Table S1: Reactions and corresponding reactions rate of the comprehensive Markov model that fits the MD simulations, or its simplified version used in the main text. For the comprehensive Markov model, rate values are only shown for $\epsilon^+_{AB}, \epsilon^-_{AA} > 6$, where Arrhenius equation applies (otherwise, the rates are directly taken from the MD simulations). We only represent the reactions where A binds C before B, but the reverse order is possible and the same rates apply.

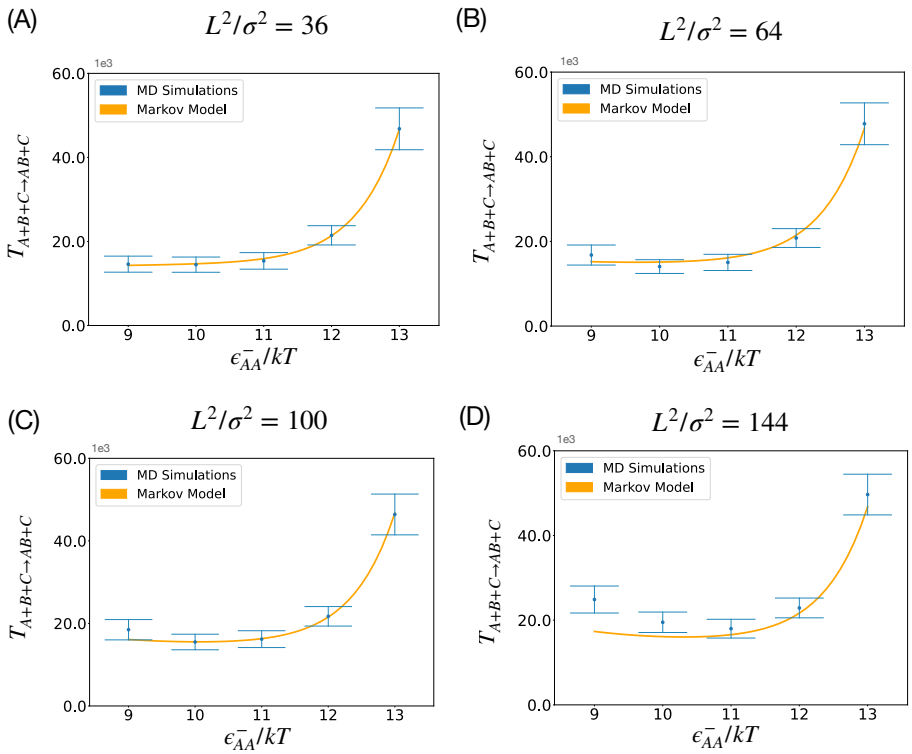

Figure S3: Mean time to form a product AB in the presence of an (auto)catalyst C for different reaction areas L^2 and interaction strengths ϵ_{AA}^{-}. These results demonstrate how the Markov model that we have derived fits quantitatively the MD simulations.

1.4 Extension to anisotropic particles

Here we show how the analysis can be extended to anisotropic particles. For simplicity, we illustrate an example of cross-catalysis, where CD catalyzes $A + B \to AB$ and AB catalyzes $C + D \to CD$, as represented in Fig. S4. There are two main distinctions compared to the case with isotropic particles.

First, diffusion is effectively longer, as it includes a rotational diffusion to orient particles with respect to each other. Formally, if the patches cover a fraction r of the particles, only a fraction r^2 of all encounter events lead to an actual interaction, resulting in $T_d^{\text{patch}} = T_d r^{-2}$. However, for patches of sizes 0.1σ, MD simulations yield $r^{-2} \approx 10$, in contrast to the anticipated $r^{-2} \approx 100$ (Fig. S5A). This reduced entropic barrier arises from the particles not diffusing away once they come into proximity with each other [10], a phenomenon of the same nature than the previously discussed difference between T_d and T_d'. This effect occurs in both 2D and 3D environments and has been extensively studied [10, 11, 12, 13].

Second, patches can position the substrates nearer to their transition state, leading to a shorter dimerization on the catalyst, represented by T_c (Fig. S5B). As previously, T_c scales with barrier but can be significantly smaller than T_d even when the later is estimated in confined areas.

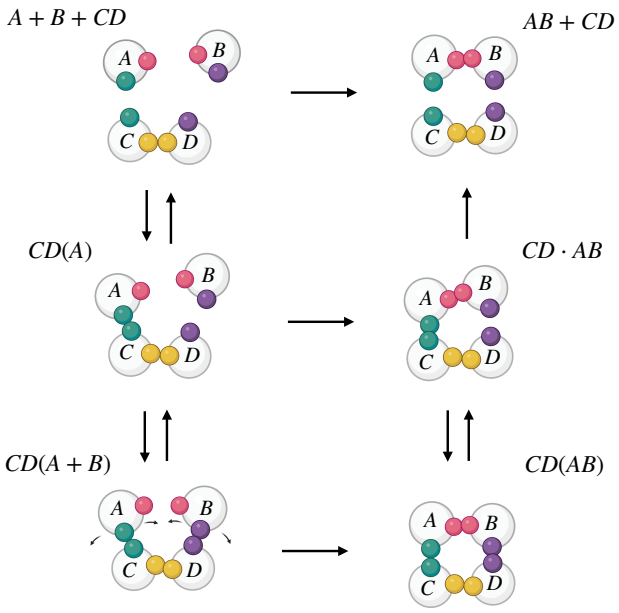

Figure S4: Cross-catalysis with anisotropic (patchy) particles. Patches of the same colors can interact one with another. The decomposition in 6 state is the same as the one discussed in the case of isotropic particles, with the difference that the autocatalyst AB is now a cross-catalyst CD.

2 Limiting barriers

2.1 Limiting barrier in the absence of product

Here we detail the derivation of the limiting barrier of the catalytic cycle for the dimerization reaction as a function of the concentration of the monomers, $[A] = [B]$, the interaction strength between particles of the same types, ϵ^-_{AA}, and the interaction barrier ϵ^+_{AB}. This derivation is based on the simplified Markov model of Table S1.

In the absence of product, we obtain the kinetic barriers for the catalytic cycle are given by Eqs. (6) and (7) in the main text:

$$G^\ddagger_1 - G_1 = -\ln[A] - \ln 2 \qquad G^\ddagger_2 - G_1 = -2\ln[A] - \epsilon^-_{AA} - \ln 2$$
$$G^\ddagger_2 - G_2 = -\ln[A] \qquad G^\ddagger_3 - G_1 = -2\ln[A] - 2\epsilon^-_{AA} + \epsilon^+_{AB}$$
$$G^\ddagger_3 - G_3 = \epsilon^+_{AB} \qquad G^\ddagger_3 - G_2 = -\ln[A] - \epsilon^-_{AA} + \epsilon^+_{AB} + \ln 2$$
$$G^\ddagger_4 - G_4 = 2\epsilon^-_{AA}.$$

The limiting barrier is the largest of these barriers. It depends on the parameters and can be determined either analytically or numerically. The limiting barrier $G^\ddagger_j - G_i$ is said to be direct if $i = j$ and indirect if $i < j$. Overall, we find the following:

At high values of $-\ln[A]$, corresponding to low substrate concentrations, the dominating barriers are indirect barriers, namely $G^\ddagger_2 - G_1$, which represents the diffusion of two substrate molecules to the catalyst, and $G^\ddagger_3 - G_1$, the diffusion of the substrate followed by a subsequent dimerization reaction. Specifically, $G^\ddagger_3 - G_1$ surpasses $G^\ddagger_2 - G_1$ when the duration of the chemical step significantly exceeds the substrate release time, $\epsilon^+_{AB} > \epsilon^-_{AA} - \ln 2$. The threshold for a to be considered "high" is determined by the conditions under which these dominating barriers are indeed larger than the other barriers, leading to $-\ln[A] > (3\epsilon^-_{AA})/2 + 1/(2\ln 2)$ and $a > \epsilon^+_{AB} + 2\ln 2$.

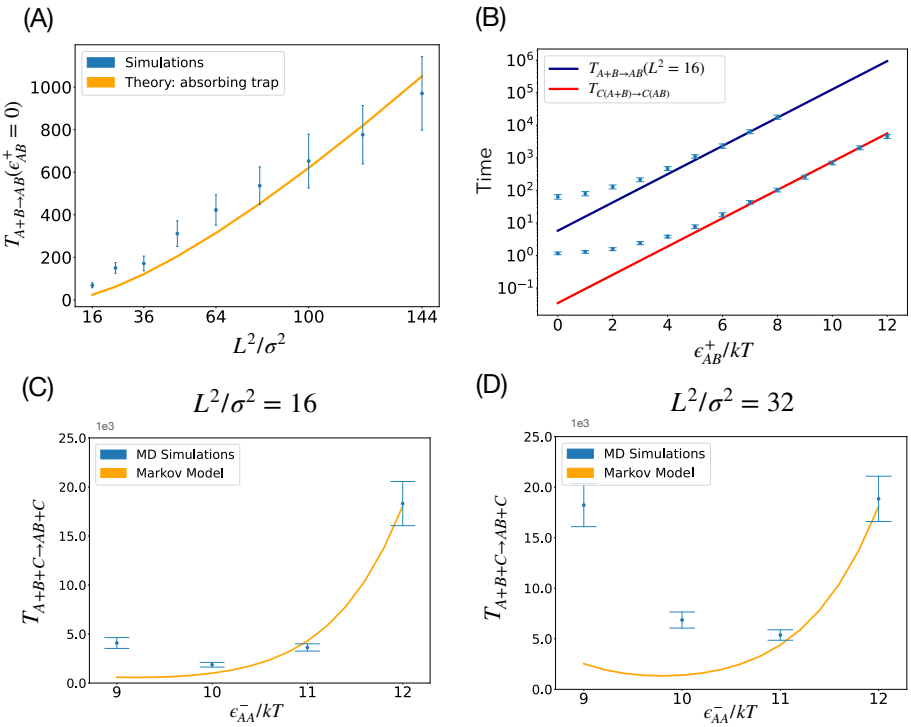

Figure S5: MD simulations and Markov models with anisotropic particles. **(A)** Mean time required for two particles, initially positioned randomly, to diffuse towards each other and interact through their patches. The analysis reveals that this time is approximately 1/10 of the diffusion time for isotropic particles. **(B)** Representation of the dimerization reaction in the bulk (purple line) or on the catalyst (red line), plotted against the interaction barrier ϵ^+_{AB} showing how the dimerization reaction on the autocatalyst occurs swiftly, since the particles are suitably oriented for interaction. **(C) - (D)** Mean times to form a product with a catalyst in the reaction vessel, as computed by both MD simulations and a Markov model for anisotropic particles.

When ϵ^+_{AB} takes high relative values, the limiting barriers are either direct or indirect barriers associated with the chemical step, $G^\ddagger_3 - G_3$, $G^\ddagger_3 - G_1$, or $G^\ddagger_3 - G_2$. In particular, the direct barrier, $G^\ddagger_3 - G_3$, dominates when the duration of the chemical step exceeds that of the release, $\epsilon^+_{AB} > 2\epsilon^-_{AA}$. This dominance also requires that the interaction strength significantly exceeds the rate of diffusion, expressed as $\epsilon^-_{AA} > -\ln[A] + \ln 2$. Conversely, in scenarios where these conditions are not met, the indirect barriers $G^\ddagger_3 - G_1$ or $G^\ddagger_3 - G_2$ dominate.

Finally, when ϵ^-_{AA} is sufficiently large, the barrier associated with product release, $G^\ddagger_4 - G_4$, dominates. These results are summarized in Fig. 1B of the main text for $\epsilon^+_{AB} = 1$.

2.2 Limiting barrier in the presence of product

In the presence of the product, three new barriers arise,

$$
\begin{aligned}
G^\ddagger_1 - G_0 &= -\ln[A] + 2\epsilon^-_{AA} + \ln[AB] - \ln 2 \\
G^\ddagger_2 - G_0 &= -2\ln[A] + \epsilon^-_{AA} + \ln[AB] - \ln 2 \\
G^\ddagger_3 - G_0 &= -2\ln[A] + \epsilon^+_{AB} + \ln[AB]
\end{aligned}
$$

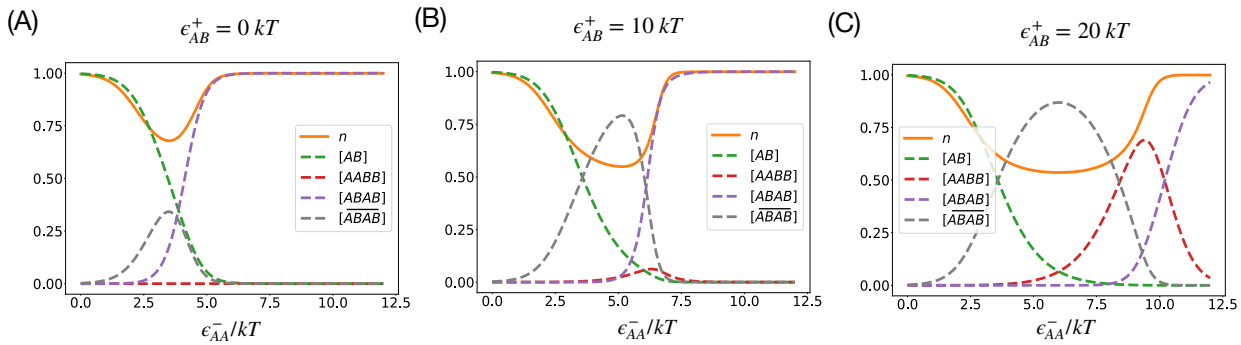

Figure S6: Reaction order and relative species concentration as a function of the interaction strength ϵ^-_{AA} for different values of the interaction barrier ϵ^+_{AB}. The reaction order is maximal ($n = 1$) when the interaction strength is either weak or strong. At intermediary strength, however, $0.5 < n < 1$, due to the presence of product inhibition (high $[\overline{ABAB}]$). We verify that $[AB] \approx [AB]_{\text{tot}}$ for weak interaction strength, and $[AB] \approx 0$ at large interaction strength.

They are equivalently written as $G_i^\ddagger - G_0 = G_i^\ddagger - G_1 + \ln[AB] + 2\epsilon^-_{AA}$ for $i = 1, 2, 3$, thus indicating that these barriers dominate the respective barriers $G_i^\ddagger - G_1$ only when $2\epsilon^-_{AA} > -\ln[AB]$, that is, for high concentration of product relative to the interaction strength. In such cases, $T_{\text{cycle}} \approx T_{\text{inhib}}$. Moreover, we find that $G_1^\ddagger - G_0$ and $G_2^\ddagger - G_0$ dominate over $G_4^\ddagger - G_4$ when $-\ln[A] > -\ln[AB] + \ln 2$ and $-2\ln[A] > \epsilon^-_{AA} - \ln[AB] + \ln 2$, that is, when the concentration of substrate is lower than that of the product. These results are summarized in Fig. 4A of the main text.

3 Growth laws

3.1 Growth regimes

Instead of a fixed concentration of free product $[AB]$ (fixed parameter $-\ln[AB]$), we may consider a fixed total concentration of product $[AB]_{\text{tot}}$, including products that interact with catalysts. The difference is illustrated in Fig. 4 of the main text showing that the limiting barrier is changed only for high values of the interaction strength ϵ^-_{AA}. This is because for small ϵ^-_{AA}, most products are in free form, $[AB] \approx [AB]_{\text{tot}}$, while for large ϵ^-_{AA}, most products are in complexes.

More quantitatively, the regime of small ϵ^-_{AA} requires $\epsilon^-_{AA} < -\ln[AB]/2$ and $\epsilon^-_{AA} - \ln[AB] + \ln 2 < -2\ln[A]$. Because increasing ϵ^-_{AA} affects the limiting barrier both directly (as per the formulas) and indirectly (through decreasing the concentration of $[AB]$), the regime of high ϵ^-_{AA} is less easy to determine precisely in general. However, in conditions where the chemical step is much longer than all other processes ($\epsilon^+_{AB} \gg -\ln[A], 2\epsilon^-_{AA}$), von Kiedrowski showed that the reaction order n can be estimated as [14]

$$n = \frac{4K_2[AB]_{\text{tot}}q^2}{8K_2cq^2 + (1+q)^2 - (1+q)\sqrt{8K_2cq^2 + (1+q)^2}}, \tag{S4}$$

where $q = 1/(K_1[A]^2)$, $K_1 = (k_1/k_{-1})^2 = e^{2\epsilon^-_{AA}}$, and $K_2 = (k_2/k_{-2})^2 = e^{2\epsilon^-_{AA}}$. From this expression, it follows that exponential growth occurs when release is limiting, that is when $K_1[A]^2 \gg \sqrt{2K_2[AB]_{\text{tot}}}$ and $K_1[A]^2 \gg 1$. We verify these different results in Fig. S6 where the reaction order is computed numerically (as per Material and Methods) as a function of the interaction strength ϵ^-_{AA} for different values of the reaction barrier ϵ^+_{AB}.

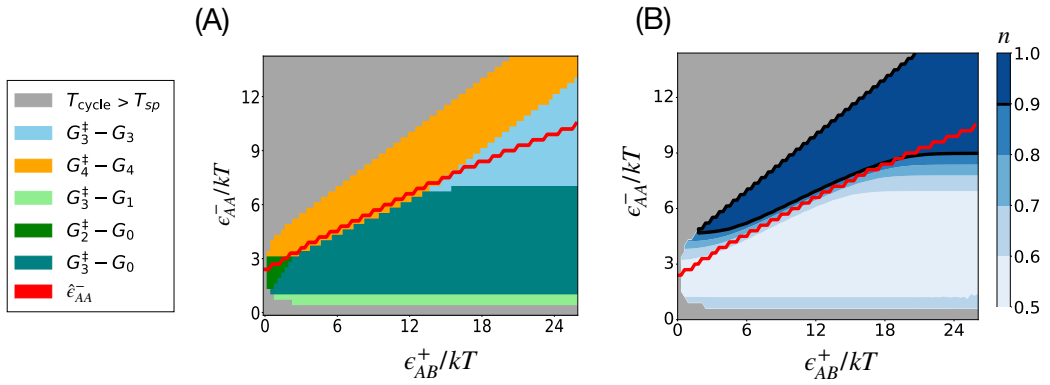

Figure S7: Relationship between k and n as a function of the interaction barrier ϵ_{AB}^+. At low interaction barrier, the interaction strength ϵ_{AA}^- that maximizes k occurs for $n \approx 0.5$. In this regime, the limiting barrier is $G_2^\ddagger - G_0$. As the interaction barrier increases, the optimal k is reached for n closer to $n = 1$. At high interaction barriers, the limiting barrier is $G_3^\ddagger - G_3$, and k and n are not in trade-off anymore. Here $[A] = e^{-4}$ and $[AB]_{\text{tot}} = e^1$.

3.2 Trade-off between the rate k and the reaction order n

Exponential growth ($n = 1$) is achieved for either low or high interaction strength ϵ_{AA}^- (Fig. S6), but maximal turnover (k^{-1}) is achieved for an intermediary interaction strength (Sabatier principle). This raises the question of a trade-off between k and n. As shown in Fig. S7B, this trade-off is present only for some values of ϵ_{AB}^+. For small values of ϵ_{AB}^+, the optimal k is achieved while $n = 1/2$, implying a clear trade-off, but for larger values of ϵ_{AB}^+, the optimal k is achieved while $n \lesssim 1$, implying a marginal trade-off, while for even larger values of ϵ_{AB}^+, the optimal k is achieved while $n = 1$, implying no trade-off.

This is rationalized by recognizing that the limiting barrier defines different regimes as a function of ϵ_{AB}^+ (Fig. S7A). For small ϵ_{AB}^+, k is optimized when $G_2^\ddagger - G_0$ is limiting, which is a barrier caused by product inhibition. For larger ϵ_{AB}^+, $G_3^\ddagger - G_0$ dominates over $G_2^\ddagger - G_0$. This barrier is also caused by product inhibition but does not depend on ϵ_{AA}^-. It is therefore minimized by minimizing $[AB]$, until the point where $G_3^\ddagger - G_0$ equates $G_4^\ddagger - G_4$, which depends on ϵ_{AA}^-. The optimal interaction strength is then found at the boundary between $G_3^\ddagger - G_0$ and $G_4^\ddagger - G_4$, corresponding to $n \lesssim 1$. For even larger ϵ_{AB}^+, k is optimized when the limiting barrier becomes $G_3^\ddagger - G_3$, which is unrelated to product inhibition, leading to $n = 1$.

3.3 Exponential growth and limiting barriers with the comprehensive Markov model

To simplify the presentation, we analyze in the main text a Markov model that is a simplified version of the Markov model obtained from the MD simulations (supplementary section 1.3). In Fig. S8, we replicate Fig. 4B-C with the more comprehensive Markov model. The comparison between Fig. S8 and Fig. 4B-C shows that the two models lead to very comparable results. The primary distinction is that a greater interaction strength ϵ_{AA}^- is necessary for (auto)catalysis to take place. Crucially, for such strong interactions, pre-factors of order 1 are negligible, and the simplified model is therefore justified.

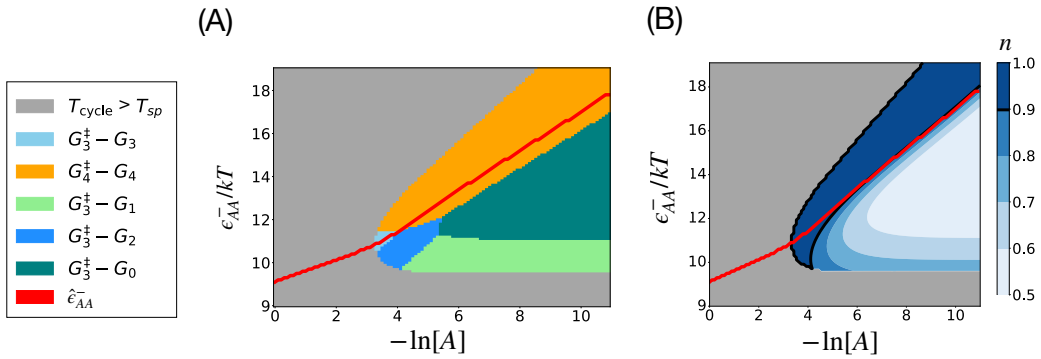

Figure S8: Limiting barriers in the presence of products. **A.** Reaction order n, as computed from simulations of the ordinary differential equations describing the specific Markov model, when fixing the total concentration of autocatalyst $[AB]_{\text{tot}}$. The results are comparable to Fig. 4C, although shifted from stronger interaction strengths (note the difference of scale for the y-axis). **B.** Limiting barriers when fixing the total concentration of autocatalyst to $[AB]_{\text{tot}} = e^{-3}$. The results are comparable to those of Fig. 4B.

Supplementary References

[1] Y. Zhang, X. He, R. Zhuo, R. Sha, J. Brujic, NC. Seeman, PM. Chaikin. Multivalent, multiflavored droplets by design. *Proc. Natl. Acad. Sci.*, 115(37):9086–9091, 2018.

[2] X. Wang, S. Ramírez-Hinestrosa, J. Dobnikar, D. Frenkel. The Lennard-Jones potential: when (not) to use it. *Phys. Chem. Chem. Phys.*, 22(19):10624–10633, 2020.

[3] F. Cui, S. Marbach, JA. Zheng, M. Holmes-Cerfon, DJ. Pine. Comprehensive view of microscopic interactions between DNA-coated colloids. *Nat. Commun.*, 13(1):2304, 2022.

[4] JA. Anderson, J. Glaser, SC. Glotzer. HOOMD-blue: A Python package for high-performance molecular dynamics and hard particle Monte Carlo simulations. *Comput. Mater. Sci.*, 173:109363, 2020.

[5] TD. Nguyen, CL. Phillips, JA. Anderson, SC. Glotzer. Rigid body constraints realized in massively-parallel molecular dynamics on graphics processing units. *Comput. Phys. Commun.*, 182(11):2307–2313, 2011.

[6] J. Glaser, X. Zha, JA. Anderson, SC. Glotzer, A. Travesset. Pressure in rigid body molecular dynamics. *Comput. Mater. Sci.*, 173:109430, 2020.

[7] FL. Vot, SB. Yuste, E. Abad, DS. Grebenkov. First-encounter time of two diffusing particles in two- and three-dimensional confinement. *Phys. Rev. E*, 105(4):044119, 2022.

[8] S. Arrhenius. Über die Reaktionsgeschwindigkeit bei der Inversion von Rohrzucker durch Säuren. *Z. Phys. Chem.*, 1889.

[9] S. Redner. *A guide to first-passage processes.* Cambridge University Press, 2001.

[10] OG. Berg. Orientation constraints in diffusion-limited macromolecular association. The role of surface diffusion as a rate-enhancing mechanism. *Biophys. J.*, 47(1):1–14, 1985.

[11] K. Šolc, WH. Stockmayer. Kinetics of diffusion-controlled reaction between chemically asymmetric molecules. II. Approximate steady-state solution. *Int. J. Chem. Kinet.*, 5(5):733–752, 1973.

[12] D. Shoup, G. Lipari, A. Szabo. Diffusion-controlled bimolecular reaction rates. The effect of rotational diffusion and orientation constraints. *Biophys. J.*, 36(3):697–714, 1981.

[13] C. Eun. Effects of the Size, the Number, and the Spatial Arrangement of Reactive Patches on a Sphere on Diffusion-Limited Reaction Kinetics: A Comprehensive Study. *Int. J. Mol. Sci.*, 21(3):997, 2020.

[14] G. Von Kiedrowski. Minimal Replicator Theory I: Parabolic Versus Exponential Growth. In H. Dugas and FP. Schmidtchen, editors, *Bioorg. Chem. Frontiers*, volume 3, pages 113–146. Springer, Berlin, Heidelberg, 1993.